JAAS

A Novel Horizontal Solution Cathode Glow Discharge Geometry for Atomic Emission Spectrometry

Journal:	*Journal of Analytical Atomic Spectrometry*
Manuscript ID	JA-ART-02-2022-000063.R1
Article Type:	Paper
Date Submitted by the Author:	01-Apr-2022

Complete List of Authors:	Hazel, Nicholas; State University of New York at Buffalo, Department of Chemistry Orejas Ibañez, Jaime; University of Oviedo, Physics Ray, Steven; State University of New York at Buffalo, Department of Chemistry

A Novel Solution Cathode Glow Discharge Geometry for Improved Coupling to Optical Emission Spectrometry

Nicholas Hazel, Jaime Orejas Ibanez, and Steven Ray*

Department of Chemistry, State University of New York at Buffalo, Buffalo, NY USA 14226

*Author to whom correspondence should be addressed.

Abstract

The Solution-Cathode Glow-Discharge (SCGD) is an atmospheric pressure glow discharge used for atomic emission spectrometry that is typically sustained between a metallic pin-anode and a liquid cathode, wherein sample solutions are introduced as a flowing stream emanating from a cylindrical capillary. A novel SCGD is reported here which sustains the SCGD plasma in a horizontal arrangement between a flat anode and a cathode constructed from a thin, rectangular capillary. This new arrangement creates a sheet-like plasma in which the negative glow of the SCGD approximates the shape of the entrance slit of a spectrophotometer,improving the efficiency of optical sampling. The analytical capability of the horizontal cathode SCGD is compared with a conventional SCGD and found to improve sensitivity and decrease limits of detection as much as 33-times for the 24 elements examined. Improvement is particularly significant for elements whose atomic emission is concentrated near the liquid cathode surface. The current/voltage characteristics and spatial distribution of atomic emission of the SCGD are reported, matrix effects associated with the design are examined, and a simple preconcentration technique for ground water analysis is also explored.

Introduction

The solution-cathode glow-discharge (SCGD) is an atmospheric pressure plasma developed for atomic emission spectroscopy (AES) which has its roots in experiments reported as early as 1887, and which was first refined for AES by Cservalfi et al[1-5]. In the modern SCGD designed for AES[3], an atmospheric pressure glow discharge is sustained in the ambient atmosphere between a metal pin anode and a liquid cathode. The sample solution to be analyzed is introduced as a flowing stream through a glass capillary to act as the liquid cathode[5]. As the solution exits the glass capillary, it is sampled directly into the plasma, where atomic and molecular emission can be measured for quantitative analysis[6, 7]. The SCGD is capable of limits of detection ranging from 0.01-1 μg/L for many elements, making it competitive with radially-viewed inductively coupled plasma atomic emission spectroscopy (ICP-AES) [8]. However, unlike ICP-AES, the SCGD requires no purified gas flows, no plasma containment chambers or nebulizers, operates with very low power consumption (<100W), requires simple DC electronics, and produces relatively simple spectra composed mainly of neutral atomic lines.

The SCGD has been used to quantitate elemental composition at trace and ultra-trace levels in a wide variety of sample types including silica colloids [9], nanoparticles[10], bottled water[11], wastewaters[12], honey[13], and wine[14]. It has also found use with hydride generation[15], water remediation[16, 17], and nanoparticle synthesis[18]. Because the SCGD-AES is a relatively nascent technique, a variety of methods and geometries have been reported to improve the analytical figures of the merit of the technique. For example, the addition of low molecular weight molecules[19, 20], surfactants [21], and different acid electrolytes[22] have been studied as a means to improve transfer of analyte into the SCGD plasma. Alternate means of solution grounding[5],

electrode geometries[23], and alternate discharge powering schemes[24] have also been examined. The use of the reversed polarity discharge (solution as anode) has also been examined as a means of improving detection limits for some elements[25, 26]. However, while a variety of different approaches to solution grounding have been reported[5, 27-29], the architecture of the discharge itself has remained essentially the same in most studies.

Our laboratory has recently constructed a novel SCGD using a rectangular capillary in order to examine both the mechanism of droplet ejection from the liquid cathode surface of the SCGD and the structure of the SCGD at the cathode spots originating from high speed plasma tendrils[30]. The use of different capillary (and anode) shapes allows the plasma structure to be changed, moving from the cone-shape discharge of the typical pin-anode SCGD to the curtain-like structure which is useful in different SCGD applications. In AES, for example, atomic emission has shown to be spatially dependent in the plasma, with molecular background emission being more pronounced in the positive column and atomic emission located predominately in the cathode glow near to the liquid surface[31-33]. This emission distribution stems from the high electric field ($>10^6$V/m) and high temperature gradient (3000K/mm) present in the cathode-glow region of the plasma[34-36]. The structure of the SCGD has also been shown to be filamentary in nature when viewed on fast timescales[37]. Since the cathode glow region generally contains the greatest atomic emission yield and little of the background species, increasing the size of the cathode glow region and more effectively capturing the radiation emitted from this region improves the sensitivity and limits of detection of a given analysis. Indeed, Schwartz et al have recently showed that SCGD limits of detection can be improved by 1.4-13.6-times by using spatially-dependent collection of SCGD emission[31].

In this work, we use the rectangular capillary geometry described previously by Orejas et al in order to produce a long, curtain shaped SCGD discharge[30]. The SCGD plasma is then rotated 90^0 from a typical SCGD orientation, such that the cathode glow of the plasma describes a thin, vertical optical slit-like emission region. This cathode emission region is the approximate shape and geometry of the spectrometer entrance slit, and thus provides more efficient coupling to the optical spectrometer and omits background from the surrounding plasma regions. Rectangular capillaries of several sizes are examined to assess the optimum parameters to be used for atomic emission spectrometry, evaluating both electrical and emission characteristics. The spatial atomic emission distribution and analytical figures of merit of 24 elements are examined, comparing the rectangular capillaries to the conventional capillary SCGD in terms of limits of detection, sensitivity, dynamic range, and measurement precision. The severity of common matrix effects are examined, and the utility of a preconcentration step to achieve environmentally relavent detection limits is demonstrated.

Experimental

A representation of the SCGD experimental setup is shown in **Figure 1**. The DC glow discharge plasma was sustained between the sample solution emanating from rectangular borosilicate capillaries (Friedrich&Dimmock, Inc, Millville NJ) of various dimensions and an 8 mm square titanium anode ground to a wedge-like pointed edge (Grade 2, 99% purity, McMaster Carr, Robbinsville, NJ). The rectangular capillaries used here have a long, thin cross-section so that the open end of the capillary forms a discharge cathode that has a 'trough' shape. The "medium sized capillary" (MC) used here had an inner capillary dimension of 0.3mm x 3mm. The flowing liquid introduced into the capillary base overflowed the sides of this trough. A list of capillary dimensions and acronyms used to reference them in the text are listed in **Table 1**. The

rectangular capillaries were set into custom 3D-printed polylactic acid (PLA) holders specific to each capillary size (Ender 5 pro, Creality). Each capillary type was then fit into an electrically grounded aluminum support structure and connected to the sample inlet tubing, ensuring reproducible location. The support structure was set atop a 3D-printed PLA base that held both capillary and anode in a horizontal arrangement, as shown in **Figure 1**. The sample solution introduced into the capillary overflowed from the capillary tip and made contact with a 1/8" diameter graphite rod, which acted as connection to electrical ground for the circuit. Excess waste solution was collected in a reservoir milled into the aluminum block.

A DC power supply (Glassman High Voltage, Series EK) operating in current-control mode was used to supply voltage through a 2KΩ, 100W ballast resistor set in series between the titanium electrode and the power supply. A ceramic insulator was used to isolate the titanium anode from the aluminum structure and electrical ground. Applied potentials between 800V-1000V supported currents from 40mA – 100mA. Discharge current was measured by the voltage drop across a 100Ω, 10W resistor placed in series with the circuit, and discharge voltage monitored using a high voltage probe (Tektronix, P6015) located between the ballast resistor and the discharge anode. Voltage and current measurements were monitored using an oscilloscope (Tektronix, TBS 1154). All experiments occurred in the ambient atmosphere. Additional images of the horizontal SCGD experimental arrangement are included as **supplemental figure 1**.

A conventional pin-type SCGD was used for comparative studies, it has been described in detail elsewhere[8]. Briefly, the pin-type SCGD plasma was sustained between a pin-type titanium anode (3/16" OD, tapered to a point) and the solution emerging from a borosilicate capillary (0.38mm ID, 1.1mm OD, Kimble Inc). The sample solution was introduced into the capillary to overflow from the capillary tip onto a graphite rod (1/8" O.D., McMaster Carr) which acted as the

circuit ground. The glass capillary was inserted into the bottom of a cylindrical teflon waste solution container, holding anode and cathode in a vertical orientation.

A peristaltic pump (Perimax 12, Spetec) was used to provide solution to both SCGD devices, and the same peristaltic pump was used to remove excess solution from the waste collection stream. Solution flow rates from 2.5mL/min to 3.0 mL/min were typically used. Sample solutions were prepared by diluting high purity 1000 mgL^{-1} standards (Sigma Aldrich, Accustandard) in aqueous 0.1M HNO_3 (Nitric acid, trace metals grade, Fisher Scientific) solution made using 18-MOhm ultrapure water (Aries water filtration). Unless otherwise noted, all samples were prepared in 0.1M HNO_3.

Emission from the SCGD was collected using a 75mm focal length quartz lens, and the plasma was imaged onto the entrance slit of a 0.3m F/4 spectrometer (Andor Shamrock 303i/300nm blaze/1200 lines/mm) equipped with a EMCCD (Andor Newton 971). The CCD was thermoelectrically cooled to -50° C and no signal gain was used. In some instances, noted in the text, a 0.35m F/6.8 monochromator (Heath EU-700) equipped with a photomultiplier tube (Hammamatsu, R928) was used for single-wavelength measurements. The resulting PMT photocurrent was amplified (Stanford SR570) and captured using a custom data acquisition program (Labview, National Instruments). The plasma support structure was placed on a movable stage that allowed a region of the plasma to be focused onto the spectrometer entrance slit. Images of the plasma were also captured with a DSLR (Nikon, D5300) using a reversed f/1.4 50mm lens and high-speed videos captures using a CMOS camera (Chronos 1.4, Kron Technologies).

Sample preconcentration experiments used home-built columns packed with 0.5g Chelex-100 styrene divinylbenzene chelating resin (BioRad, Inc). The homemade columns were made from 5-inch sections of Nalgene tubing (1/4 inch OD, 1/8 inch ID). Glass wool was packed at each

end of the column to contain the resin. Each column was prepared off-line by rinsing with 18MΩ water followed by a 3mL aliquot (6.0mL/min for 30s) of 2.0M NH_4Ac equilibration solution. A 500mL sample solution aliquot was introduced to the column at a rate of 6.0 mL/min, and then the column was rinsed with a 3mL aliquot of 0.05M NH_4Ac (6.0mL/min for 30s). Preconcentrated sample was eluted using 0.5M HNO_3[38]. Eluted sample was delivered to the SCGD via a "T" valve that connected to the main flow sustaining the plasma. SCGD flow was maintained at 3.0mL/min while the 0.5M HNO_3 flow was introduced at 1.0mL/min.

Results and Discussion

The rectangular SCGD geometry was developed to control the cathode surface area in a way that limits the width of the glow discharge structure along one axis, forming the SCGD cathode glow into an optically-thin ribbon-like discharge. Because the entendue of the monochromator should be the limiting element of optical throughput in the experiment, it follows that radiant flux and AES signal are maximized by selectively sampling the spatial region of greatest atomic emission yield in the SCGD. Atomic emission from elements analyzed in the SCGD is often concentrated in the cathode glow region, and thus the ribbon-like structure corresponds well with the entrance slit of the monochromator. Indeed, Schwartz and coworkers have shown that detection of atomic emission based on defined regions of interest within the SCGD increases S/N[31]. In addition, many authors have noted that AES signal increases with increasing SCGD discharge power until the discharge collapses through arc formation[8]. Recent studies have shown that the current density at the cathode surface remains approximately constant regardless of cathode size or shape, and thus increasing SCGD power is achieved by increasing cathode size[30].

In **Figure 2**, several images of the rectangular SCGD operating under typical conditions in a horizontal orientation are shown, wherein each image shows the plasma upon introduction of a 100µg/mL solution of In (Figure 2A), Tl (Figure 2B), Y (Figure 2C), and 10 µg/mL Li (Figure 2D). The short-exposure images (1/4000s) clearly show the distinct structure of the GD (i.e. dark space, negative glow, positive column) as noted in other examples[31], as well as the presence of individual and distinct plasma tendrils that cover a portion of the cathode surface[30]. The glow covers approximately 50% of the entire cathode surface under these conditions, and thus has a current density of 49mA/mm^2 , which agrees with prior measurements[30]. Each image in **Figure 2** also reveals the spatial distribution of atomic emission, which is typically greatest in the cathode glow region (e.g. Figure 2A). As reported by Schwartz et al[34], the tendril nature of the SCGD plasma is further emphasized because atomic emission only occurs in the channel of the plasma tendrils, which move across the liquid cathode surface in a rapid, stochastic manner. High speed videos illustrating this motion of the horizontal SCGD are available in **supplemental figure 2**. The distribution of atomic emission is element and species dependent, for example, yttrium oxide emission is observed in the positive column, as might be expected based on the formation of oxides, and Li emission occurring both in the cathode glow and the positive column as also observed elsewhere[2]. Additional comparative images of the conventional vertical SCGD analyzing the same solutions are included as **supplemental Figure 3.**

Both the geometry and orientation of the SCGD and the spatial distribution of atomic emission have a significant influence on the spectrometric analysis. In **Figure 3**, images of both the horizontal and conventional SCGD are shown alongside the AES spectroscopic line profile observed at the polychromator CCD camera. In Figure 3A and 3E, the dotted rectangular box placed on each image reflects the spatial region being imaged onto the spectrometer entrance slit.

In Figure 3E, the conventional SCGD orients the sampling volume between anode and cathode, and thus the spectral line profile represents an optical image of emission between the two electrodes, as shown elsewhere[29]. By contrast, in Figure 3A the horizontal SCGD orients the slit image along the cathode glow, capturing emission across the cathode surface. Both experiments here used the same measurement and optical imaging conditions (i.e. lens, slit width, magnification).

The optical spectra shown in Figure 3 compare the spatial emission distribution of Tl (Tl(I) 535.0nm), Cs (Cs(I) 852.1nm), Ag, (Ag(I) 338.2nm, Ag(I) 328.0nm), and background molecular emission from N_2 ($C^3\Pi_u \rightarrow B^3\Pi_g$, 337nm) captured when using the conventional SCGD with the horizontal SCGD reported here. Each of the spectra is presented using the same monochrome scale, slit width, and integration time (2.5s), with the dotted lines used to denote the orientation of the cathode surface to the image in each instance (i.e. Figure 3B and 3F). In Figure 3A-D the horizontal SCGD (Type: MC) shows atomic emission along the length of the slit height, while the atomic emission observed from the vertical SCGD is concentrated at lower vertical slit height. The consequence of the discharge orientation are apparent. Using a 1.4x magnification the conventional vertical SCGD images only 3% of the cathode glow area (1.1mm dia. cathode). By contrast, the horizontal orientation images the entire cathode glow region onto the entrance slit of the monochromator. Interestingly, as shown in Figure 3B, greater emission intensity is often observed near the bottom of the horizontal SCGD cathode (Figure 3B, C), which is most likely due to the effect of gravity-driven flow of the liquid surface. Prior studies have shown that atomic emission from a rectangular capillary surface is symmetric when the rectangular SCGD is oriented vertically [30].

The spatial distribution and intensity of nitrogen vibronic emission from the two SCGD structures is also different. Comparing Figures 3D and 3H, it is clear that the background emission from nitrogen N_2 ($C^3\Pi_u \rightarrow B^3\Pi_g$, 337nm) is greater in the conventional SCGD. In addition, the observed continuum background is greater overall (approximately 50%-100% greater), although the magnitude is dependent on the spectral region. A series of comparative optical spectra showing this difference in continuum are included as **supplemental Figures 4A-I,** and background measurements and background RSD values for several elemental emission lines are listed in **supplemental table 1**. The molecular OH ($A^2\Sigma^+ \rightarrow X^2\Pi$, 306nm) and N_2 ($C^3\Pi_u \rightarrow B^3\Pi_g$, 337nm) background are observed in both the cathode glow and positive column of the discharge[36], however, nitrogen emission also originates from the ambient atmosphere and is therefore typically most prominent in the positive column of the discharge[7]. Since the horizontal SCGD does not sample emission from the positive column or anode glow structures, both continuum and discrete background sources are reduced throughout the optical spectrum. The presence of some residual N_2 emission in **Figure 3D** is likely due to the discontinuous tendril nature of the discharge (see **Figure 2**), and nitrogen intrusion between the tendrils as they move along the solution surface contributes to the background in the cathode glow.

Effect of Discharge Current and Solution Flow Rate

Figure 4A compares the current – voltage relationships for the standard round capillary with each horizontal capillary SCGD. In each case the current-voltage relationship was linear and similar, with the largest area cathode (type:XLC) able to sustain a discharge over the greatest range of applied currents (30-105mA, 841-989V) while the smallest cathode area (type: SC) was stable over the smallest range (50-90mA, 971-1040V). The conventional capillary (type: RC) was stable over the range from 40-100mA (910-1026V). Applied power at the same discharge voltage also

decreased for larger cathode areas in the horizontal SCGD examples. The noise power spectra of the discharge as related to each structure were similar, and similar to those reported previously[30]. In contrast to our experience using similar rectangular SCGD structures in a vertical arrangement, the maximum currents achieved by the horizontal SCGD were similar to the conventional SCGD, despite the larger cathode area[8, 30]. This difference may be due to the effect of the gravity-fed solution flow, as noted in **Figure 3**. **Figure 4A** and prior reports have suggested that the SCGD operates in the abnormal glow discharge regime, which is not entirely true. Prior studies have shown that the discharge operates in a pseudo-normal mode in the sense that current density at the cathode remains constant with increasing discharge potential. As discharge current increases, additional points of contact between the plasma and solution surface increase the effective cathode area [30]. Images and high-speed videos of the horizontal capillary SCGD operating under different discharge currents are included as **supplemental figure 5** and **supplemental figure 6**. These images depict the stochastic motion of the discharge tendrils and increase in number as the discharge current increases, as reported elsewhere[30].

Figure 4B shows the effect of discharge current on observed emission from a 1 mg/L solution of Li (Li(I) 670.7nm) for each of the SCGD geometries studied. As reported in previous studies, increasing the SCGD discharge current uniformly increases the total atomic emission observed[39, 40]. The rate of increase in emission intensity vs current is greatest for the horizontal capillary structures as compared to the conventional SCGD and somewhat linear over the range examined. The same response is common to most of the analyte elements examined; **supplemental figure 7A-E** show a similar response of atomic emission on discharge current for the elements Cs (Cs(I) 852.1nm), In (In(I) 451.1nm), Ga (Ga(I) 417.2nm), and Pb (Pb(I) 405.7nm). In some instances, signal RSD does increase for each SCGD geometry with increasing discharge

currents. The influence of discharge current on both continuum background, the molecular nitrogen bandhead ($C^3\Pi_u \rightarrow B^3\Pi_g$, 337nm), emission from OH ($A^2\Sigma^+ \rightarrow X^2\Pi$, 306nm), and from H_α 656.3nm are included as **supplemental figures 8A-D**. Here, most continuum and molecular background increases with increasing discharge current for both the horizontal and conventional SCGD, although some background components (e.g. H_α) do show a markedly different response.

The effect of sample flow rate on observed emission from Ag (Ag(I) 338.2nm) and Mg (Mg(I) 285.2nm) for several SCGD geometries (type: RC, MC) are presented in the **Figure 4C.** Generally, sample flow rates between 1.4 – 5.2mL/min produced a stable plasma for these structures, with slight differences due to cathode area evident in increased flow rates possible for larger area capillaries (e.g. type: MC). The horizontal SCGD showed a relatively flat sensitivity response to changes in solution flow rate, while the conventional capillary (type: RC) showed a large dependence on solution flow rate. The background emission in both capillaries followed the same trends, for example, OH emission in the horizontal SCGD increased only slightly 12% from 1.4- 5.8mL/min, while OH background from the conventional capillary followed the same dependence as the Ag emission shown in Figure 4C and was approximately twice the amplitude as the horizontal SCGD. A very small increase in applied potential (2-5%) was observed with increasing flow rates in both RC and MC structures. Voltage curves and charts of the effect of flow rate on molecular background species are included as **supplemental figure 9**.

Analytical Figures of Merit and Spatial Emission Distribution

Calibration curves for the element In obtained using the horizontal SCGD are compared with the conventional SCGD in **Figure 5**. In each case, the sensitivity obtained using the horizontal SCGD is markedly greater as compared to the conventional design, with the SC and LC structures providing highest sensitivity. Notably, the SC and LC strucutres have the smallest

cathode areas and most narrow width (see Table 1), which effectively limits the SCGD structure into a sheet-type discharge. Solution flow rates were 2.5mL/min for the RC and 3.0mL/min for each rectangular capillary, and a 3mm discharge gap and 80mA discharge current was used in all cases. Each calibration curve showed linear response over 4 orders of magnitude.

Calibration curve sensitivity and limits of detection (LOD) determined for In(In(I) 451.1nm), Pb (Pb(I) 405.7nm), Al (Al(I) 396.1nm), and Ga(Ga(I) 417.2nm) using each of the different SCGD geometries are compiled in **Table 2.** These results show that all of the horizontal SCGD capillaries (type: SC, MC, LC, XLC) provide greater sensitivity and improved limits of detection as compared to the conventional approach. With the horizontal SCGD (type: SC), In (In(I) 451.1nm) sensitivities (defined by the slope of the calibration curve) improved by 10-times, Pb (Pb(I) 405.7nm) improved by 5-times, Al (Al(I) 396.1nm) improved by 1.2-times, and Ga (Ga(I) 417.2nm) by 2.6-times, as compared to the conventional SCGD (type: RC). As a consequence of improved sensitivity and decreased background levels, the horizontal SCGD (type: SC) showed LODs (calculated as $3\sigma_{background}$/sensitivity[41, 42]) that improved for In (In(I) 451.1nm) by 35-times, for Pb (Pb(I) 405.7nm) by 10-times, for Al (Al(I) 396.1nm) by 2.4-times, and for Ga (Ga(I) 417.2nm) LOD by 3.3-times. These improvements observed are dependent on the specific horizontal capillary (type: SC, MC, LC, XLC) as well as element. Generally, however, the smallest cathode area (Type: SC) showed the greatest improvement in sensitivity and lowest LODs. Each of the calibration curves studied were within the linear range for the respective line, (i.e; 0.5-25 mg/L).

The element-dependent improvement in LODs and sensitivity are a result of the spatial dependence of emission of different elements in the SCGD structure. Normalized spatial emission profiles collected between the cathode and anode for the different SCGD geometries are shown in

Figure 6. In these plots, the cathode surface is located at a distance of 0.5 mm and the tip of the tungsten anode is located at a distance of 3.5 mm in each plot, although emission extends slightly beyond these points as the plasma sheath wraps around the tips of both electrodes. The spatial distributions of emission are segmented into four groups as previously defined by Schwartz et [31]. These groups are termed "narrow," (Figure 6A), "semi-narrow," (Figure 6B), "semi-diffuse," (Figure 6C), and "diffuse", (Figure 6D). These labels reflect the profile of the emission between cathode and anode. The "narrow" grouping contains elements whose emission is predominantly contained in the cathode glow region and drops off at rapidly above this region. "Semi-narrow" elements emit most strongly in the cathode glow as well, however emission from these elements decreases at a slower rate into the positive column. Atomic emission from "semi-diffuse" elements decrease at an even slower rate, and elements in the "diffuse" category emit broadly across the length of the plasma. As shown in **Figure 6**, most elements studied have maximum emission in the cathode glow of the plasma, and emission intensity generally drops 60-95% of this value in the positive column. As a consequence, sensitivity for these elements is improved by imaging the entire cathode region. Interestingly, the "diffuse" category contains predominantly emission lines below 300nm and each shows a very broad spatial distribution that reaches a maximum in the midway between anode and cathode. It appears that this may be due to optical aberrations resulting from low wavelength emission lines and the use of a quartz lens, as reported previously[31].

Several elements (e.g. Li and Sr) display a double-humped spatial distribution with nearly the same emission intensity in the positive column and cathode glow[2]. Supplemental figure 10 illustrates that lines from the same elements follow the same spatial distribution, as noted by other researchers, suggesting a common excitation condition[43]. Spatial emission distributions of the major background species present in the SCGD including H_α (656.3nm), H_β (486.1nm), and the

bandheads of molecular N_2 (337nm), and OH (306nm), can be found in **supplemental figure 11**. In agreement with others SCGD reports, H_α and H_β emit predominately close to the solution surface and very little in the positive column, whereas emission from OH is more diffuse and primarily in the positive column. N_2 (337nm) is more intense in the cathode glow region however it also presents intense emission in the positive column near the anode glow. Overall, these profiles are similar to those found by other reports [2, 33, 36]. As shown in **supplemental figure 12**, these spatial patterns do not change significantly with increased discharge current or solution flow rate.

Since the spatial distribution of atomic emission influences how much atomic emission is collected from the cathode glow, or not observed from the positive column, it is likely that element-dependent sensitivity and LODs are due to spatial distribution of emission. The 24 elements listed in **Table 3** are segregated into the "narrow" group (4) "semi-narrow" group (5), "semi-diffuse" group (9), and "diffuse group (6). The "narrow" spatial distribution group, 8/8 showed improved sensitivity and 7/8 showed improved LODs. The "semi-narrow" group had 7/8 lines show improved sensitivity and 8/8 showed improved LODs, the "semi-diffuse" group 8/14 lines show improved sensitivity, and 11/14 showed improved LODs, and the "diffuse" group had only 2/7 lines with improved sensitivity but 7/7 showed improved LODs. The sensitivity enhancement is a reflection of the concentration of emission at the cathode region, and thus the 'narrow' emission group showed the greatest improvement in sensitivities. The improvement in LODs seen here is a combination of increased sensitivity and a lower, and more stable background.

A comprehensive list of calibration curves and limits of detection determined with three capillaries (type: RC, SC, MC) are available in **supplemental table 2**. Overall, the smallest horizontal capillary (type: SC) provided best analytical results, with 24/36 (66%) lines showing improved sensitivity and 32/36 (88%) showing improved LODs. The LOD improvement was

element-dependent, with significant improvement observed for some elements (e.g. In (In(I) 451.1nm) (35-times), Ag (Ag(I) 328.0nm) (20-times), Cs Cs(I) 852.1nm) (17-times)) and more modest improvements for other elements. LODs reported here are similar to, or better than, those reported recently in a comprehensive literature review[5]. A comparison of signal RSD and background values for these SCGD geometries are also available in **supplemental table 2**. Signal RSD values achieved here (0.1-2.5% RSD) are similar to or better than those achieved using the conventional SCGD [5]. As noted previously, background spectral emission was notably lower when using these horizontal SCGD systems (e.g. 52% decrease at Cd (Cd(I) 228.8nm), but varied across the optical spectrum.

A linear dynamic range extending 3-5 orders of magnitude was achieved for most elements using the horizontal SCGD, which is similar to the conventional SCGD and previous reports[44, 45]. However, deviation from linearity at higher concentrations was found to be more severe for the horizontal SCGD as compared to the conventional SCGD in some cases. For example, the (type: RC, SC, MC, LC, XLC) calibration curves for Li (In(I) 451.1nm) and Ag (Ag(I) 338.2nm) provided as **supplemental figures 13 A** and **13B**. In Figure 5, In (In (I) 451.1nm) shows a linear response across the whole studied concentration range (0.1 – 50mg/L), however, both Ag and Li show a negative deviation from linear response at lower concentration (e.g. 25mg/L Ag) as compared to the conventional SCGD. This limit of linearity deviation might be caused by self-absorption**,** however, the horizontal SCGD are optically thin relative to the conventional SCGD. More likely, deviation from linearity reflects the influence of emission from the positive column that is not observed in the horizontal SCGD. Particulary for those elements in the "semi-narrow" or "defuse" groups tend to show deviation of this type because of the significant emission that occurs in the positive column.

Matrix effects

Matrix effects, and particularly those due to easily ionizable elements (EIE), are widely observed in SCGD-AES[46]. The suppression observd upon addition of 50mg/L and 100mg/L solutions of Na to several different atomic emission lines for different elements are shown in **Figure 7A.** Generally, addition of up to 100mg/mL of interferent changes the observed emission from the horizontal SCGD by 1-10% , which is similar to the change observed in the conventional SCGD (see **supplemental figure 13)** and reported previously. The effect of the addition of 50mg/L and 100mg/L solutions of several matrix interferents (Na, In, Mg, Ni, Fe) on net emission from In (In(I) 451.1nm) when using a horizontal capillary (type: MC) are plotted in Figure 7B. The most significant decrease observed was a 40% suppression upon addition of 100mg/L Li, however, it is worth noting that this may reflect the greater molar concentration of the Li as compared to the other interferents. The matrix effect severity on different emission lines of In (I) and Ga were found to be similar between the conventional capillary and the horizontal capillary (type: MC), and are included in **supplemental figure 14.** It was found that matrix suppression at higher interferent concentration could be more severe in the horizontal SCGD. For example, Ag emission suppression upon addition of higher concentrations of Na was found to be more severe for the horizontal SCGD as compared to the conventional SCGD, as shown in F**igure 7B**. This disparity may be due to the influence of EIE effect in the negative glow of the discharge, although no spatial shifts of the SCGD were observed.

Preconcentration

Preconcentration is an effective means of achieving the low limits of detection that are required for many environmental monitoring applications. Such approaches are particularly attractive for use with the SCGD, since the system operates using a continuous flowing sample

stream and has been shown to be useful for flow-injection analysis previously[47]. Preconcentration approaches using graphene oxide for Pb [48] and mesoporous silica for Cr and Hg[49, 50] have been reported previously in conjunction with the SCGD.

In order to demonstrate the utility of the approach for environmentally relevant elements, a simple resin-based FIA system was constructed to study preconcentration of Pb and Cu in water samples[47]. Home-built preconcentration columns containing 0.5g of Chelex-100 were prepared, and each column was loaded with 500mL of sample solution. Preconcentrated Pb and Cu were eluted off each column by directing the 1.0mL/min 0.5M HNO_3 SCGD flow through a 6-port valve for a period of 2 minutes to ensure complete elution. Limits of detection were calculated based on maximum peak-height of the the elution peak for each sample. The LODs for Cu (Cu(I) 324.7nm) were improved from 11ppb (type: SC) to 0.054ppb (type: SC + Preconcentration), and Pb (Pb(I) 368.3nm) LODs improved from 36ppb (type: RC) to 0.72ppb (type SC + Preconcentraiton). The LODs for Pb and Cu determined with preconcentration are well below the current EPA drinking water action limits of 15ppb (Pb) and 1300ppb (Cu)[51]. **Supplemental Table 3** lists the LODs obtained. While such schemes can be applied to almost any AES method, they are particularly attractive for use with a SCGD-AES in a quasi-continuous monitoring application.

Conclusion

An alternative SCGD architecture based on a rectangular liquid electrode has been developed and shown to provide improved sensitivity and LODs for most elements studied with the SCGD. Analytical performance was found to vary with capillary geometry and element. The medium size capillary (type: MC) had a maximum LOD improvement of 10-times and maximum sensitivity improvement of 6-times, and an average improvement in LODs of 2.5-times and an average improvement in sensitivity of 1.3-times for the 24 elements studied. The smallest

horizontal capillary (type: SC) showed a maximum LOD improvement of 34-times and maximum sensitivity improvement of 11-times, and led to an average improvement in LOD of 10-times and a sensitivity improvement of 1.9-times compared to the conventional capillary for the 24 elements studied. When combined with a simple off-line preconcentration scheme, LODs for Pb and Cu in ground waters were demonstrated that were well below EPA drinking water action limits.

The reason for these element-dependent improvements in LOD and sensitivity was shown to be dependent on the spatial distribution of emission within the discharge. Because the horizontal SCGD is designed to collect emission from the cathode and negative glow of the GD only, as opposed to across the entire GD structure as occurs in conventional SCGD, improvement in LOD and sensitivity is most pronounced for elements that exhibit the highest proportional emission in the cathode and negative glow regions. Elements were classed according to their spatial emission profile between cathode to anode, and it was shown that improvements coorelated broadly within these classes. Limits of detection were also shown to improved because background emission and continuum arising from the positive column of the SCGD is ignored, thereby decreasing background noise. Conversely, the fact that the positive column of the discharge is not observed may also be responsible for slight differences between the approaches. Matrix effects from EIE elements were found to be similar between the horizontal SCGD and conventional SCGD up to moderate matrix concentrations, but were worse for horizontal SCGD systems at higher matrix concentration. In addition, several elements were observed to have a decreased limit of linearity at the higher concentration portion of the calibration curve, in part because emission from the positive column was not observed.

Acknowledgements: This work was supported in part by the National Science Foundation under Grant No. (CHE-1622531) and in part by the State University of New York at Buffalo. The authors

gratefully acknowledge the contribution of the UB Department of Chemistry Mass Spectrometry Facility, the UB CAS Machine Shop, and the UB Department of Chemistry Electronic Shop. The authors thank Indiana University and Professor Gary Hieftje for the donation and loan of some of the equipment used in this study. The authors also thank and acknowledge the ICP Information Newsletter and Professor Ramon Barnes for support. The authors particularly thank Professor Barnes for his stalwart support of the atomic spectrometry community over a period of five decades, acting as a role model, teacher, and sage for generations of researchers and students.

Data Availability: Data and STL files available on request from the authors.

References

1. J. Gubkin, *Annalen der Physik*, 1887, **32**, 2.
2. M. R. Webb, F. J. Andrade, G. Gamez, R. McCrindle and G. M. Hieftje, *Journal of Analytical Atomic Spectrometry*, 2005, **20**.
3. P. M. T. Cserfalvi, P. Apai, *Journal of Physics D: Applied Physics*, 1993, **26**, 2184-2188.
4. J. E. Foster, *Physics of Plasmas*, 2017, **24**.
5. P. Pohl, P. Jamroz, K. Greda, M. Gorska, A. Dzimitrowicz, M. Welna and A. Szymczycha-Madeja, *Anal Chim Acta*, 2021, **1169**, 338399.
6. A. J. Schwartz, J. T. Shelley, C. L. Walton, K. L. Williams and G. M. Hieftje, *Chem Sci*, 2016, **7**, 6440-6449.
7. P. Mezei and T. Cserfalvi, *Sensors (Basel)*, 2012, **12**, 6576-6586.
8. P. Pohl, P. Jamroz, K. Swiderski, A. Dzimitrowicz and A. Lesniewicz, *TrAC Trends in Analytical Chemistry*, 2017, **88**, 119-133.
9. Z. Wang, A. J. Schwartz, S. J. Ray and G. M. Hieftje, *J. Anal. At. Spectrom.*, 2013, **28**, 234-240.
10. N. Hazel, J. Orejas and S. J. Ray, *Spectrochimica Acta Part B: Atomic Spectroscopy*, 2021, **176**.
11. P. Zheng, N. Wang, J. Wang, X. Mao, C. Lai, C. Zhong, W. Li and Y. Luo, *Microchemical Journal*, 2019, **151**.
12. C. Huang, Q. Li, J. Mo and Z. Wang, *Anal Chem*, 2016, **88**, 11559-11567.
13. K. Greda, P. Jamroz, A. Dzimitrowicz and P. Pohl, *Journal of Analytical Atomic Spectrometry*, 2015, **30**, 154-161.
14. K. Greda and P. Pohl, *Food Chem*, 2022, **371**, 131178.
15. J. Cheng, Q. Li, M. Zhao and Z. Wang, *Anal Chim Acta*, 2019, **1077**, 107-115.
16. C. Sugama, F. Tochikubo and S. Uchida, *Japanese Journal of Applied Physics*, 2006, **45**, 8858-8863.
17. R. Wajahat, A. Yasar, M. Zakaullah, A. B. Tabinda, A. Ikhlaq, Y. Mahfooz and S. G. Bhatti, *Desalination and Water Treatment*, 2021, **225**, 225-230.
18. A. Dzimitrowicz, A. Motyka, P. Jamroz, E. Lojkowska, W. Babinska, D. Terefinko, P. Pohl and W. Sledz, *Materials (Basel)*, 2018, **11**.
19. C. G. Decker and M. R. Webb, *Journal of Analytical Atomic Spectrometry*, 2016, **31**, 311-318.
20. D. E. Moon and M. R. Webb, *Journal of Analytical Atomic Spectrometry*, 2020, **35**, 1859-1867.
21. K. Greda, P. Jamroz and P. Pohl, *Talanta*, 2013, **108**, 74-82.
22. J. Yu, S. Yang, D. Sun, Q. Lu, J. Zheng, X. Zhang and X. Wang, *Microchemical Journal*, 2016, **128**, 325-330.
23. P. Zheng, Y. Luo, J. Wang, Y. Yang, Q. Hu, X. Mao and C. Lai, *Microchemical Journal*, 2022, **172**.
24. R. Huang, Z. Zhu, H. Zheng, Z. Liu, S. Zhang and S. Hu, *Journal of Analytical Atomic Spectrometry*, 2011, **26**.
25. K. Greda, K. Swiderski, P. Jamroz and P. Pohl, *Anal Chem*, 2016, **88**, 8812-8820.
26. K. Greda, S. Burhenn, P. Pohl and J. Franzke, *Talanta*, 2019, **204**, 304-309.
27. K. Świderski, P. Pohl and P. Jamróz, *Journal of Analytical Atomic Spectrometry*, 2019, **34**, 1287-1293.
28. J. Wang, P. Tang, P. Zheng and X. Zhai, *Journal of Analytical Atomic Spectrometry*, 2017, **32**, 1925-1931.
29. T. s. Cserfalvi and P. l. Mezei, *Journal of Analytical Atomic Spectrometry*, 2003, **18**.
30. J. Orejas, *Spectrochimica Acta Part B: Atomic Spectroscopy*, 2021, **181**.
31. A. J. Schwartz, S. J. Ray, G. C. Y. Chan and G. M. Hieftje, *Spectrochimica Acta Part B: Atomic Spectroscopy*, 2016, **125**, 168-176.
32. M. R. Webb, G. C. Y. Chan, F. J. Andrade, G. Gamez and G. M. Hieftje, *Journal of Analytical Atomic Spectrometry*, 2006, **21**.

33. P. Zheng, W. Li, J. Wang, N. Wang, C. Zhong, Y. Luo, X. Wang, X. Mao and C. Lai, *Analytical Letters*, 2019, **53**, 693-704.
34. A. J. Schwartz, S. J. Ray, E. Elish, A. P. Storey, A. A. Rubinshtein, G. C. Chan, K. P. Pfeuffer and G. M. Hieftje, *Talanta*, 2012, **102**, 26-33.
35. T. Cserfalvi and P. Mezei, *Journal of Analytical Atomic Spectrometry*, 2005, **20**.
36. P. Mezei, T. Cserfalvi and L. Csillag, *Journal of Physics D: Applied Physics*, 2005, **38**, 2804-2811.
37. N. Hazel, J. Orejas and S. Ray, *Journal of Applied Physics*, 2021, **129**.
38. J. Sondergaard, G. Asmund and M. M. Larsen, *MethodsX*, 2015, **2**, 323-330.
39. P. Jamroz, K. Greda and P. Pohl, *TrAC Trends in Analytical Chemistry*, 2012, **41**, 105-121.
40. Y.-A. W. Mohammad A. Mottaleb, Hyo-Jin Kim, *Microchemical Journal*, 2001, **69**, 219-230.
41. P. W. J. M. Boumans, *Spectrochimica Acta Part B: Atomic Spectroscopy*, 1991, **46**, 917-939.
42. S. Ershadi and A. Shayanfar, *J AOAC Int*, 2018, **101**, 1212-1213.
43. G. C. Chan and G. M. Hieftje, *Anal Chem*, 2013, **85**, 50-57.
44. T. Kántor and A. Bartha, *Spectrochimica Acta Part B: Atomic Spectroscopy*, 2015, **113**, 119-125.
45. W. T. C. P. B. Stockwell, N. Brahma, *Journal of Automatic Chemistry* 1996, **18**, 153-162.
46. G. C. Y. Chan and W.-T. Chan, *Spectrochimica Acta Part B: Atomic Spectroscopy*, 2003, **58**, 1301-1317.
47. A. M. Massadeh, A.-W. O. El-Rjoob and S. A. Gharaibeh, *Water, Air, & Soil Pollution*, 2020, **231**.
48. J. Mo, L. Zhou, X. Li, Q. Li, L. Wang and Z. Wang, *Microchemical Journal*, 2017, **130**, 353-359.
49. Q. Li, Z. Zhang and Z. Wang, *Anal Chim Acta*, 2014, **845**, 7-14.
50. J. Ma, Z. Wang, Q. Li, R. Gai and X. Li, *J. Anal. At. Spectrom.*, 2014, **29**, 2315-2322.
51. EPA Website, https://www.epa.gov/dwreginfo/lead-and-copper-rule, (accessed December 2021).

Figure 1

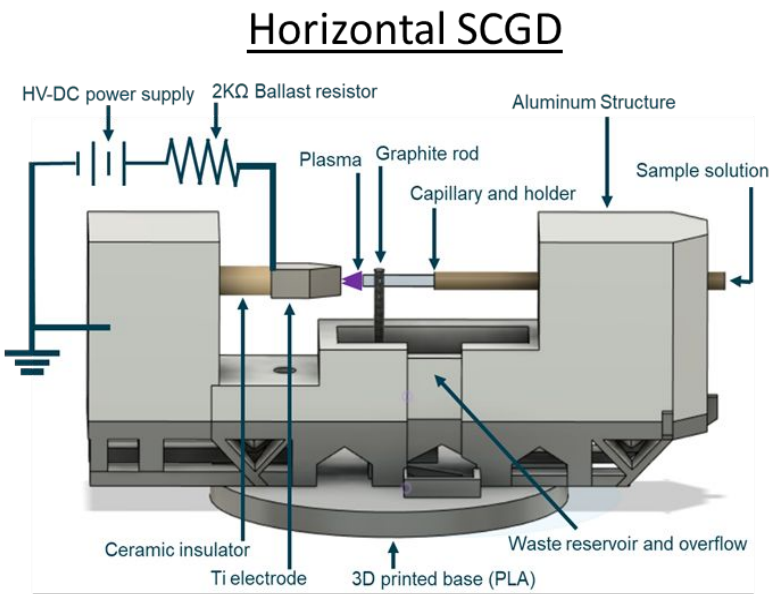

Figure 1: Schematic diagram of the horizontal capillary SCGD

Figure 1: Schematic diagrams of the horizontal capillary SCGD

Figure 2

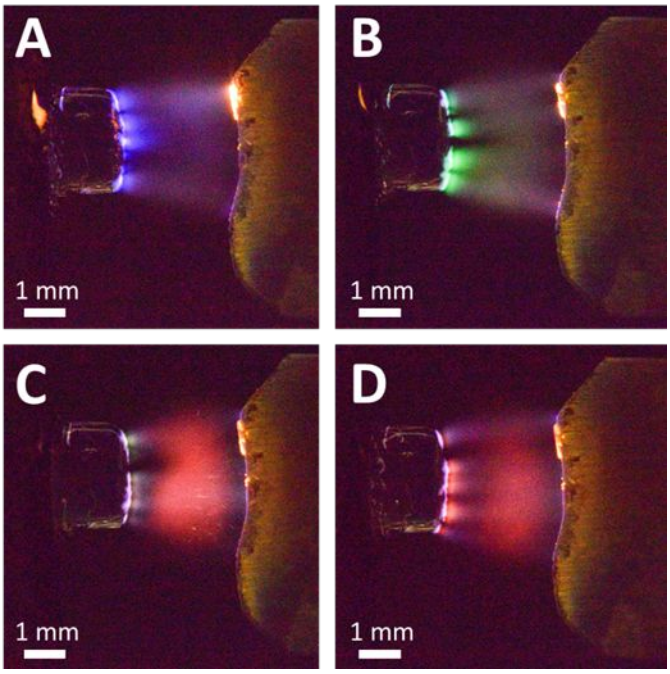

Figure 2: High-speed photos of the horizontal SCGD sampling various elements (3.0mL/min, 85mA, 3mm discharge gap, 1/4000s shutter speed). **A**) 100mg/L In, **B**) 100mg/L Tl, **C**) 100mg/L Y, **D**) 10mg/L Li.

Figure 3

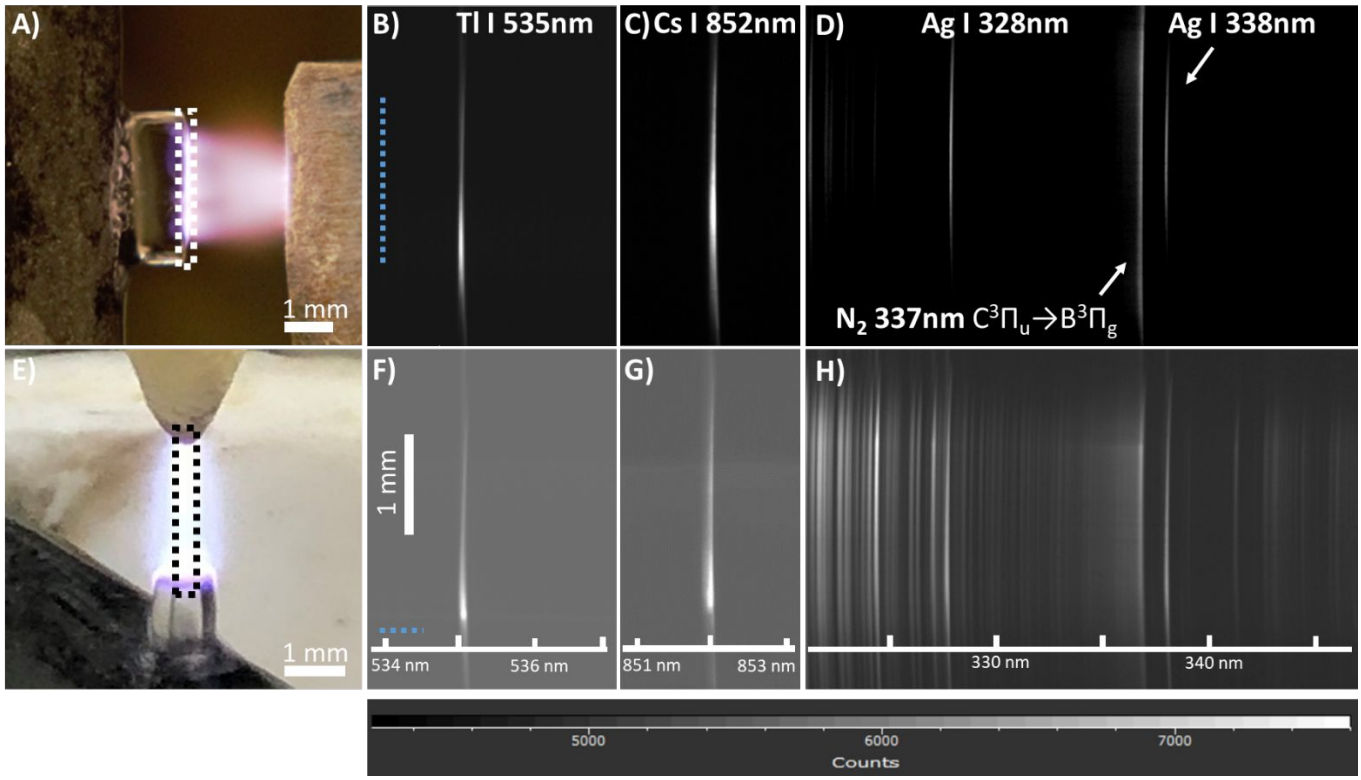

Figure 3: Spectrometric atomic emission comparison of the horizontal SCGD and conventional SCGD. A) Image showing orientation of the horizontal SCGD and accompanying emission line profiles of B) Tl I 535nm, C) Cs 852nm, and D) N_2 337nm; E) Image showing orientation of the conventional SCGD and accompanying emission line profiles of F) Tl I 535nm, G) Cs 852nm, and H) N_2 337nm.

Figure 4

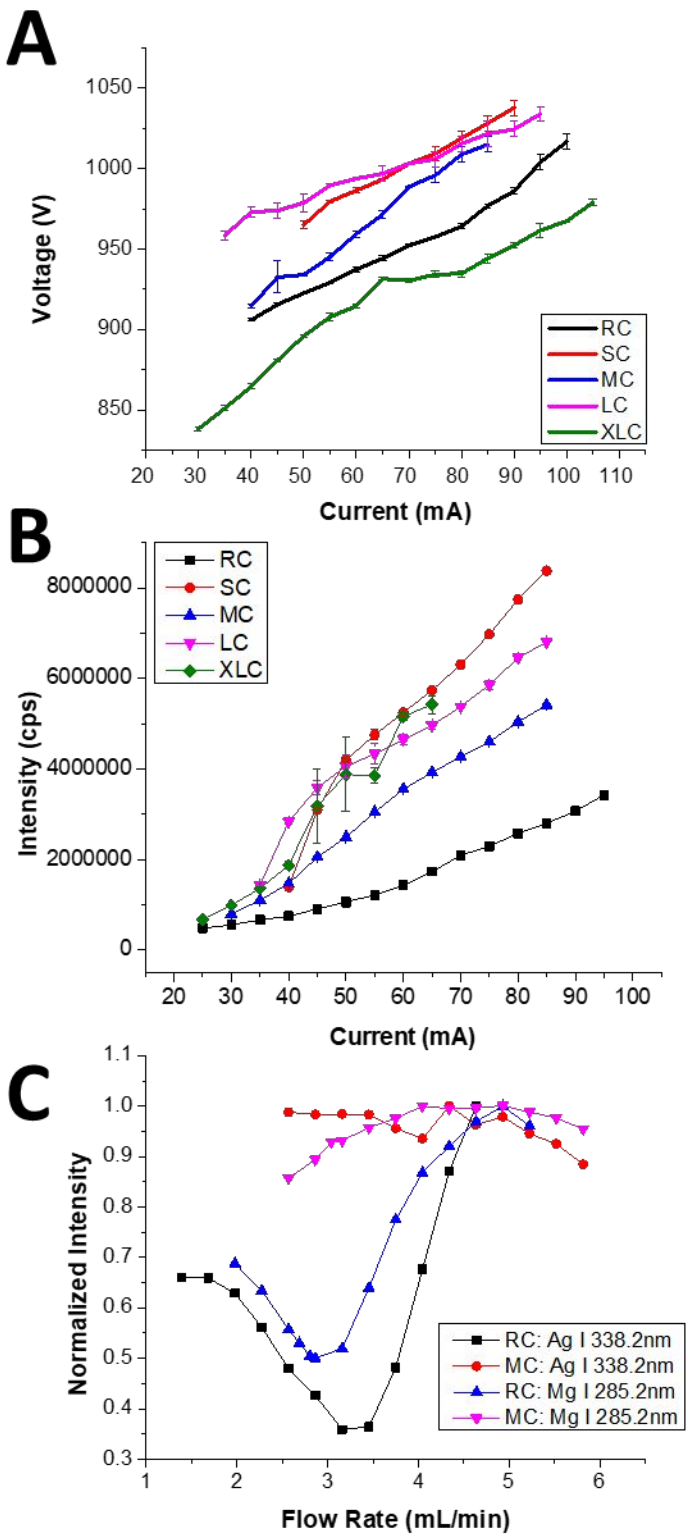

Figure 4: Comparison of horizontal SCGD and conventional SCGD operating parameters. **A**) Current-voltage curves obtained with each capillary. **B**) Dependence of atomic emission (Li I 670.7nm) on discharge current. **C)** Comparison of normalized emission from 1mg/L Ag I 338.2nm and 10mg/L Mg I 285.2nm at different sample flow rates.

Figure 5

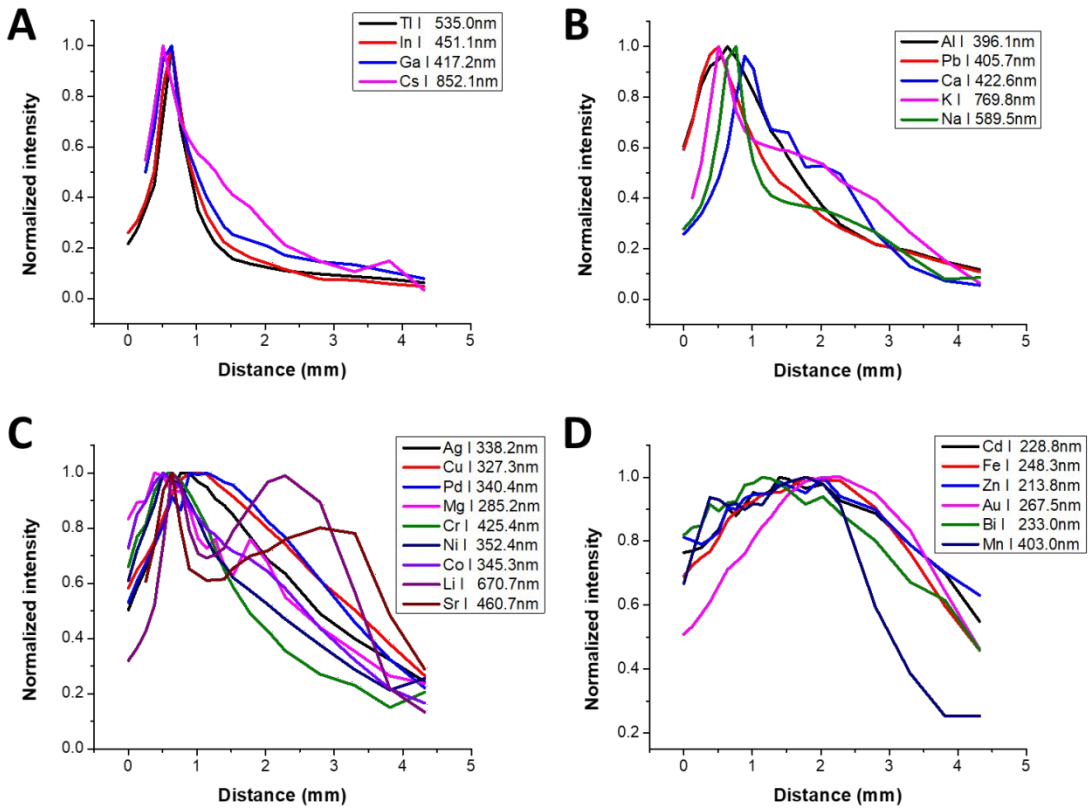

Figure 5: Normalized spatial atomic emission profiles for each element studied grouped by spatial distribution pattern. **A**) "Narrow" group. **B**) "Semi-narrow" group. **C**) "semi-diffuse" group. **D**) "diffuse" group.

Figure 6

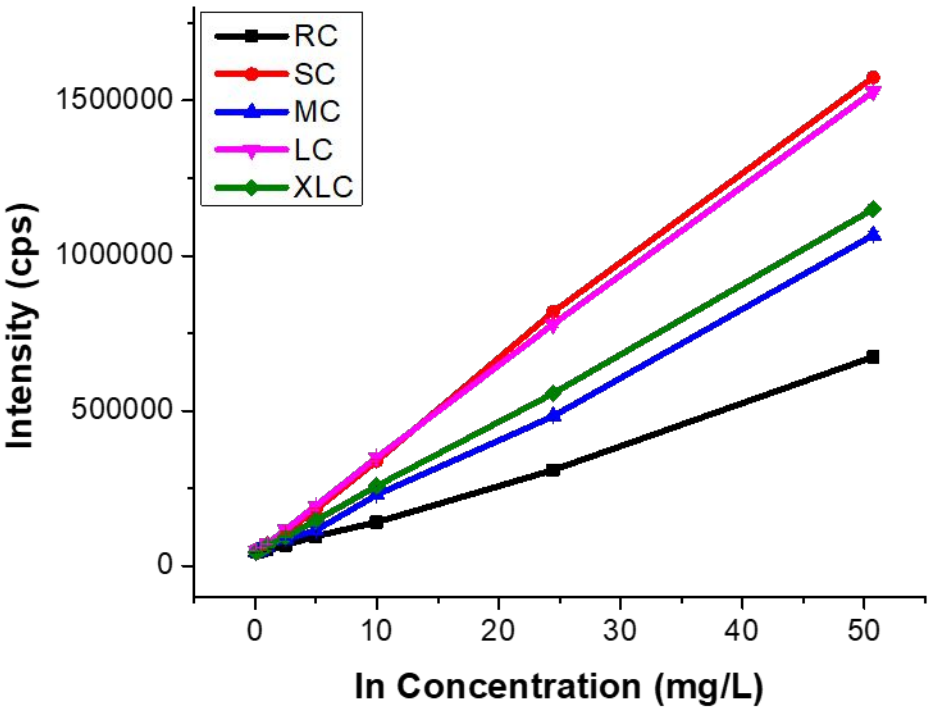

Figure 6: Calibration curves of: **A**. In 451.1nm, in 0.1M HNO_3 observed with the RC and each horizontal capillary. Solution flow rates were 2.5mL/min for the RC and 3.0mL/min for each rectangular capillary. In all cases, a 3mm discharge gap, 80mA discharge current, 50µm spectrometer slit.

Figure 7

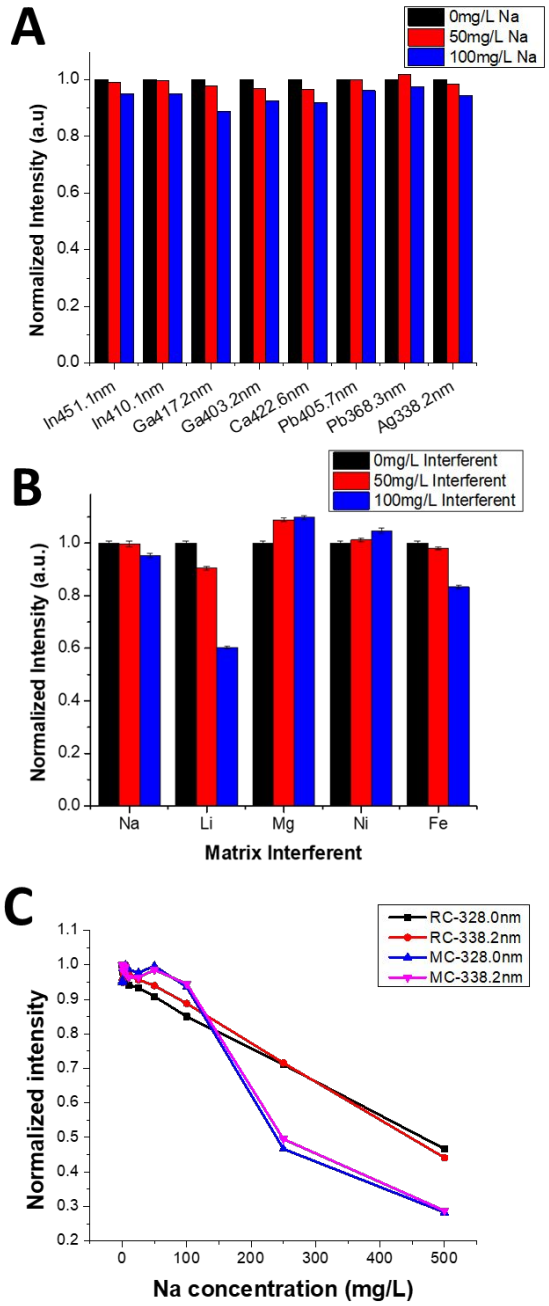

Figure 7: Matrix interferences in the horizontal SCGD. The discharge gap was 3mm, applied current was 80mA, flow rate for the RC was 2.5mL/min, horizontal capillary (MC) flow rate was 3.0mL/min. **A**) Effect of sodium on net emission from several analytes and emission lines. **B**) Effect of several different matrix interferents on net emission from 1 mg/L In (I) 451.1nm. **C**) The effect of larger concentrations of Na on emission from 1 mg/L Ag (I) 338.2nm and Ag (I) 328.0nm with the RC and MC.

Table 1

Capillaries		ID (mm)	OD (mm)	Area (mm)
Round	"RC"	0.38	1.1	0.95
Small	"SC"	0.2 x 2	0.49 x 2.15	1.05
Medium	"MC"	0.3 x 3	1.04 x 3.34	3.47
Large	"LC"	0.2 x 4	0.51 x 4.14	2.11
Extra Large	"XLC"	0.3 x 4	1.31 x 4.42	5.79

Table 1: Dimensions of each capillary studied

Table 2

	In I 451.1nm Slope (cps/mg/L)	LOD (ppb)	Pb I 405.7nm Slope (cps/mg/L)	LOD (ppb)	Al I 396.1nm Slope (cps/mg/L)	LOD (ppb)	Ga I 417.2nm Slope (cps/mg/L)	LOD (ppb)
RC	14600	86	871	1100	613	1030	19800	20
SC	154000	2.5	4400	110	745	420	51900	6.0
MC	87900	8.4	3400	180	936	220	25900	25
LC	132000	2.6	3700	130	801	560	50500	8.4
XLC	69900	5.5	2660	230	659	600	21700	16

Table 2: Results of calibration curves of In I 451nm, Pb I 405nm, Al I 396nm, and Ga I 417nm with each of the capillaries studied. Each element was studied with the same acquisition settings, a discharge gap of 3mm, and an applied current of 80mA. The RC used a sample flow rate of 2.5mL/min while each rectangular capillary used a 3.0mL/min sample flow rate.

Table 3

			Round Capillary		Small Capillary	
	Element	Wavelength	Slope (cps/mg/L)	LOD (ppb)	Slope (cps/mg/L)	LOD (ppb)
Narrow	In	451.1nm	14600	86	155000	2.5
	Tl	377.5nm	42000	31	76000	6.0
	Cs	852.1nm	94000	135	186000	7.8
	Ga	417.2nm	19800	20	51900	6.0
Semi-Narrow	Pb	368.3nm	863	799	4080	36
	Al	396.1nm	614	1020	745	423
	Ca	422.6nm	5440	63	3800	46
	Na	588.9nm	3880000	2.6	5610000	0.4
	K	766.4nm	1440000	30	2690000	0.9
Semi Diffuse	Ag	338.2nm	66500	16	75200	1.0
	Pd	340.4nm	12600	12	11500	16
	Cu	324.7nm	24800	92	61400	11
	Mg	285.2nm	154000	8.9	279000	7.5
	Li	670.7nm	723000	45	1630000	5.6
	Sr	460.7nm	2490	425	1600	193
	Cr	357.8nm	604	248	235	465
	Ni	341.4nm	1920	61	1440	54
	Co	345.3nm	1550	155	1069	85
Diffuse	Cd	228.8nm	4750	113	6490	8.1
	Zn	213.8nm	3860	122	3360	20
	Fe	248.3nm	1400	372	939	117
	Au	267.5nm	3580	184	2840	56
	Bi	223.0nm	137	5980	95	514
	Mn	403.0nm	1200	561	1650	89

Table 3: Comparison of conventional SCGD and horizontal SCGD based on calibration curves of each element and line, segmented into category according to spatial distribution of atomic emission.